Effect of resonant magnetic perturbations on particle confinement

Q. Yu and S. Günter

Max-Planck-Institut für Plasmaphysik, EURATOM Association, 85748 Garching, Germany

The effect of externally applied resonant magnetic perturbations (RMPs) on plasma particle transport is investigated based on the two fluid equations. It is found that, depending on the frequency and direction of plasma rotation, the RMP of a moderate amplitude can either increase or decrease the plasma density gradient around the corresponding rational surface. The local density profile flattens only for a sufficiently large RMP.

PACS: 52.30.Ex, 52.35.Vd, 52.55.Dy, 52.65.Kj

1. Introduction

Resonant magnetic perturbations (RMPs) have important effects on tokamak plasmas such as generating magnetic islands inside the plasma (mode penetration) [1-8], changing the plasma rotation velocity and locking sufficiently large magnetic islands [1,9-13], and mitigating edge localized modes [14].

One puzzle arising from the experimental results is the effect of RMPs on plasma confinement. Externally applied RMPs degrade tokamak particle confinement in some experiments. While improved confinement by RMPs of moderate amplitude was however observed in others[1,15,16], a phenomenon not well understood as it contradicts to the conventional understanding that the magnetic island generated by a penetrated RMP would flatten the local plasma density profile and degrade the particle confinement. The difference in tokamak wall conditioning and the role of the stochastic magnetic field in the plasma edge have been suggested as the possible explanations [1,15]

As the particle transport is a basic issue in plasma physics and is very important for a fusion reactor, the effect of RMPs on the particle confinement is investigated in this paper using the (reduced) two fluid equations. A new mechanism affecting the particle confinement by a RMP is found.

2. Model and analysis

The large aspect-ratio tokamak approximation is utilized. The magnetic field is defined as $\mathbf{B}=B_{0t}\mathbf{e}_t-(k_t/k_\theta)B_{0t}\mathbf{e}_\theta+\nabla\psi\times\mathbf{e}_t$, where ψ is the helical flux function, $k_\theta=m/r$ and $k_t=n/R$ are the wave vector in $\mathbf{e}_\theta$ (poloidal) and $\mathbf{e}_t$ (toroidal) direction, r and R are the minor and the major radius, m and n are the poloidal and toroidal mode numbers of the helical field, and the subscript 0 denotes an equilibrium quantity. The plasma velocity is given by $\mathbf{v}=v_{||}\mathbf{e}_{||}+\nabla\phi\times\mathbf{e}_t$, where ϕ is the stream function.

The two fluid equations utilized here include the mass conservation equation, the

generalized Ohm's law, and the equation of motion in the perpendicular (after taking $\mathbf{e}_t\cdot\nabla\times$) and the parallel (to magnetic field) direction. Normalizing the length to the minor radius a, the time t to the resistive time $\tau_R=a^2\mu_0/\eta$, the helical flux ψ to aB_{0t}, $\mathbf{v}$ to a/τ_R, and the electron density n_e to its value at the magnetic axis, these equations become [8,17]

$$\frac{dn_e}{dt} = d_1\nabla_{\|} j - \nabla_{\|}(n_e v_{\|}) + \nabla_{\perp}(D_{\perp}\nabla_{\perp} n_e) + S_n, \tag{1}$$

$$\frac{d\psi}{dt} = E_0 - \eta j + \Omega\nabla_{\|} n_e, \tag{2}$$

$$\frac{dU}{dt} = -S^2\nabla_{\|} j + \mu\nabla_{\perp}^2 U + S_m, \tag{3}$$

$$\frac{dv_{\|}}{dt} = -c_s^2\nabla_{\|} P/n_e + \mu\nabla_{\perp}^2 v_{\|}, \tag{4}$$

where $d/dt=\partial/\partial t+\mathbf{v}_{\perp}\cdot\nabla_{\perp}$, j is the parallel plasma current density, η the normalized resistivity, E_0 the equilibrium electric field, $U=-\nabla_{\perp}^2\phi$ the plasma vorticity, S_n the particle source, and S_m the poloidal momentum source leading to an equilibrium poloidal plasma rotation. $d_1=\omega_{ce}/\nu_e$, ω_{ce} and ν_e are the electron cyclotron and the collisional frequency, $\Omega=\beta d_1$, $\beta=4\pi P_e/B_{0t}^2$, $P=P_e+P_i$, P_e (P_i) is the electron (ion) pressure, $S=\tau_R/\tau_A$, where $\tau_A=a/V_A$ is the toroidal Alfven time. c_s, μ and $D_{\perp}$ are the normalized ion sound velocity, plasma viscosity, and perpendicular particle diffusivity. A constant electron temperature is assumed, and the cold ion assumption is made.

When the amplitude of the RMP is sufficiently small, the $\mathbf{v}_{\perp}\cdot\nabla n_e$ and $\nabla_{\|}(n_e v_{\|})$ terms in Eq. (1) can be neglected (will be shown to be true in Fig. 1), and Eq. (1) is reduced to

$$d_1\nabla_{\|} j + \nabla_{\perp}(D_{\perp}\nabla_{\perp} n_e) + S_n = 0 \tag{5}$$

in the steady state. The equilibrium electron density, n_{e0}, is given by $\nabla_{\perp}(D_{\perp}\nabla_{\perp} n_{e0})=-S_n$. Away from the rational surface at $r=r_s$, Eq. (3) ensures $\nabla_{\|} j=0$ due to the large S number for tokamak plasmas.

In the inner region around r_s, however, $\nabla_{\|} j$ is finite to balance the plasma inertia and viscous

force. In this region the radial gradient of parallel plasma current density perturbation, j_1, is much larger than that of the radial magnetic field perturbation, b_{1r}, and in the lowest order one finds $\nabla_{\|}j \approx b_{1r}j_1'$, where the prime is for the radial gradient, the subscript 1 denotes perturbed quantities, and all quantities in Eqs. (1)-(5) and in the derivation are in the dimensionless form. Integrating Eq. (5) along the minor radius and averaging over flux surfaces, one has

$$(\Delta n_e)' = -0.5(d_1/D_\perp)(b_{1r}j_1^* + b_{1r}^* j_1), \tag{6}$$

where $\Delta n_e=(n_{e,0/0}-n_{e0})$, $n_{e,0/0}$ is the m/n=0/0 component of n_e, and the superscript * refers to the complex conjugated part. Eq. (6) can be easily solved at $r=r_s$. With the perturbed helical flux $\psi_1 \sim \exp[i(-\omega t+m\theta+n\phi)]$, in the lowest order it is found from Eq. (2) that

$$j_1(r_s) = i(\omega - \omega_{E0} - \omega_{*e0})\psi_1/\eta \tag{7}$$

at $r=r_s$, where ω is the mode frequency, $\omega_{E0}=(mV_\theta/r+nV_t/R)$ is the frequency due to the equilibrium plasma rotation velocity in the poloidal (V_θ) and the toroidal (V_t) directions. $\omega_{*e0}=V_{*e0}m/r$ is the frequency due to the electron diamagnetic drift, and $V_{*e0}=-p_e'/n_eeB_{0t}$. Utilizing equation (7), Eq. (6) becomes

$$(\Delta n_e)' = -(d_1/D_\perp)(m/r)(\omega - \omega_{E0} - \omega_{*e0})|\psi_1|^2/\eta \tag{8}$$

at $r=r_s$. The mode frequency is given by the applied RMP frequency, and $\omega=0$ for a static RMP. Putting back the dimensional parameters into Eq. (8), one finds

$$r_s(\Delta n_e)'/n_e = d_1(\omega_{*e0}r_s^2/D_\perp)(1-\omega_0)|b_{1r}/B_{0t}|^2/m \tag{9}$$

for $\omega=0$, where $\omega_0 \equiv -\omega_{E0}/\omega_{*e0}$, and the same length or time units are used for the parameters in (9). $\omega_0>0$ refers to the plasma rotation in the ion drift direction (plasma current direction for a toroidal rotation). Eq. (9) shows that a RMP of a single helicity can change the local electron density gradient. The density gradient decreases ($|n_e'/n_e|$ increases in the standard case where the equilibrium density gradient is negative) for $\omega_0>1$, while in the opposite limit $(\Delta n_e)'>0$.

In addition to the change in the local electron density gradient, the electromagnetic torque

due to the applied RMP drives the plasma rotation frequency ω_E to approach the negative electron diamagnetic drift frequency ($\omega_E \approx -\omega_{*e}$) [10]. Assuming that the viscous force is larger than the plasma inertia, with a derivation similar to those shown above, the relative change of the rotation frequency is found to be

$$\Delta\omega/\omega_{E0} \approx (\tau_R V_A^2/\mu)[(w/a)(r/R)/q]^2(1/\omega_0 - 1)|b_{1r}/B_{0t}|^2 \quad (10)$$

for a toroidal plasma rotation with $\omega=0$ and $\Delta\omega << \omega_{E0}$ [10], where $\Delta\omega=(\omega_E-\omega_{E0})$, $w=4[(b_{1r}Rq)/(B_{0t}nq')]^{1/2}$ is the magnetic island width under the constant ψ assumption, and q is the safety factor. Eq. (9) predicts a significant change in the electron density gradient only under the condition

$$(\Delta\omega/\omega_{E0})/[(\Delta n_e)'/(n_e/r)] << 1, \quad (11)$$

which turns out from Eqs. (9) and (10) to be

$$(D_\perp/\mu)(\omega_{ci}/\omega_{E0})m[w/(qR)]^2 << 1, \quad (12)$$

where ω_{ci} is the ion cyclotron frequency. If ω_E and ω_{*e} are significantly different from ω_{E0} and ω_{*e0}, then the ω_{*e0} and the $(1-\omega_0)$ terms in Eq. (9) should be replaced by ω_{*e} and $(1+\omega_E/\omega_{*e})$, respectively. In the opposite limit of (12), a small static RMP leads to $\omega_E \approx -\omega_{*e} \approx -\omega_{*e0}$ before a significant change in the electron density [10]. One therefore expects a change in the density profile rather than the rotation frequency for smaller islands and larger values of q and ω_{E0}. For a deuterium plasma with $B_{0t}=2.5$T, $\omega_{E0}=10^4 s^{-1}$, $w=0.01a$, $q=3$, $R/a=3$, $m=6$, and $D_\perp=0.2\mu$, the left hand side of (12) takes a value 0.018.

3. Numerical results

To compare with analytical results discussed above and to look further into the regime with a large RMP amplitude, Eqs (1)-(4) are solved simultaneously using the initial value code TM1, which has been used earlier for modelling drift tearing modes and neoclassical tearing modes [8,13,17].

The calculations are performed for a single helicity RMP with m/n=2/1, being taken into account by the boundary condition

$$\psi_{2/1}|_{r=a} = \psi_a a B_{0t} cos(m\theta+n\phi), \quad (13)$$

where ψ_a describes the normalized m/n=2/1 helical magnetic flux amplitude at r=a. The radial magnetic field perturbation at r=a is given by $b_{1r}=-m\psi_a B_{0t} sin(m\theta+n\phi)$.

The input parameters are based on TEXTOR experimental parameters. A monotonic q profile is used with the q=2 surface located at $r_s=0.628a$ [5,9]. The m/n=2/1 tearing mode is stable for $\psi_a=0$. The toroidal magnetic field is $B_{0t}=2.5T$, the plasma minor and major radius are a=0.47m and R=1.75m. The following parameters, $S=1.97\times10^8$, $\Omega=6.3\times10^4$, $c_s=1.2\times10^7(a/\tau_R)$, $d_1=2.5\times10^8$, and $D_\perp=4.2(a^2/\tau_R)$ are used in calculations except mentioned elsewhere.

Assuming $\mu=5D_\perp$, one finds $\mu=21(a^2/\tau_R)$ in normalized units. In TEXTOR experiments the plasma rotation is essentially toroidal [5,9], while in Eqs. (1)-(4) due to large aspect ratio approximation only the poloidal rotation is included, so that a larger plasma viscosity, $\mu=2.1\times10^3(a^2/\tau_R)$, is used in our calculations for a reasonable balance between the electromagnetic and viscous force. This is based on the following reasons [1,11,13]: (a) The electromagnetic force in the toroidal direction is smaller by a factor $(n/m)(r_s/R)$ than that in the poloidal direction. (b) To have the same mode frequency due to the plasma rotation, the toroidal rotation velocity should be $(m/n)(R/r_s)$ times larger than the poloidal one. These two effects lead to a relative larger viscous force compared to the electromagnetic force for the toroidal rotation case by a factor $[(m/n)(R/r_s)]^2$, which is of the order 10^2.

The radial profiles of $(\Delta n_e)'/(n_0/a)$ in steady state, obtained by directly solving Eqs. (1)-(4), are shown by solid curves in Fig. 1 for (1) $\omega_0=3.7$ with $\psi_a=2.54\times10^{-5}$, and (2) $\omega_0=-2.7$ with $\psi_a=2.9\times10^{-5}$, where n_0 is the value of n_{e0} at r=0. The corresponding magnetic island widths are w/a=0.0122 and 0.0117. The dotted curves show the $(\Delta n_e)'/(n_0/a)$ value calculated from Eq. (6),

with b_{1r} and j_1 obtained from the numerical results. It is seen that the dotted curves are close to the solid ones. The difference from the numerical results is caused by the nonlinearity due to higher harmonics. The dashed curve shows the radial profile of $n_{e0}'/(n_0/a)$. Fig. 1 indicates that for a small island, $(\Delta n_e)'$ is positive (negative) around the rational surface for ω_0=-2.7 (ω_0=3.7) in agreement with Eq. (9). Away from the rational surface $(\Delta n_e)'$=0 as expected.

The radial profiles of the (normalized) m/n=0/0 component of the electron density, $n_{e,0/0}/n_0$, in steady state are shown in Fig. 2 for ω_0=3.7 with ψ_a=2.54× 10^{-5}, 10^{-4}, 2×10^{-4}, and 6×10^{-4} (solid curves). The corresponding island widths are w/a=0.0122, 0.0866, 0.107, and 0.176, and the screening factors, defined here as the ratio between the m/n=2/1 component of ψ at the rational surface obtained from the numerical result and that from the vacuum assumption, are found to be 0.234, 3.00, 2.28, and 2.06 respectively. The dotted curve shows the unperturbed profile of n_{e0}/n_0. With increasing ψ_a, the electron density first increases across the rational surface, forming a kind of pedestal there and reaching the maximum at $\psi_a\approx10^{-4}$. The value of $(1+\omega_E/\omega_{*e})$ at $r=r_s$ changes from -0.500 for ψ_a=2.54× 10^{-5} (unpenetrated case) to -0.0547 for $\psi_a=10^{-4}$ (penetrated case). The smaller $|1+\omega_E/\omega_{*e}|$ together with the larger island width maintains the increased electron density as well as the changed plasma rotation velocity profile for the penetrated case. The local plasma rotation frequency changes little for ψ_a=2.54× 10^{-5} and by about 20% for $\psi_a=10^{-4}$. For an even larger ψ_a (2×10^{-4}), the electron density begins to decrease and becomes smaller than n_{e0} for $\psi_a=6\times10^{-4}$. In this stage the plasma rotation frequency significantly decreases (ω_E/ω_{*e0}=-0.52 at $r=r_s$ for ψ_a=6× 10^{-4}a), which results in a corresponding small ω_{*e} (ω_{*e}/ω_{*e0}=0.473) or local electron density gradient, and the ion sonic motion and convective transport are also found to be important. In tokamak experiments the RMP results from both the intrinsic machine error field and externally applied helical field, with the magnitude of ψ_a ranging from 10^{-5}- 10^{-3} [1-5, 15,16].

For the plasma rotation in the electron drift direction with ω_0=-2.7, the radial profiles of $n_{e,0/0}/n_0$ in steady state are shown in figure 3 with ψ_a=2.9×10^{-5}, 3×10^{-5}, 10^{-4}, and 6×10^{-4}. The corresponding island widths are w/a=0.0117, 0.0640, 0.0907, and 0.183, and the screening factors are 0.187, 5.4225, 3.284, and 2.22, respectively. The dotted curve shows again the n_{e0}/n_0. With increasing ψ_a, the electron density first decreases, and the local electron density gradient changes from the usual negative value to a positive one in agreement with Eq. (9). For a sufficiently large ψ_a (6×10^{-4}), the local density profile nearly flattens. Numerical calculations confirm the analytical prediction that the local electron density is increased by a static RMP of moderate amplitude for ω_0>1, but is decreased for ω_0<1. The effect of RMPs on the plasma density gradient is larger for a larger value of $|\omega_0-1|$ with an appropriate value of ψ_a as expected from (9) and (12).

The effect of the parameter d_1 on the $n_{e,0/0}/n_0$ profile in steady state is shown in Fig. 4 with ψ_a=1×10^{-4}. The solid (dashed) curves correspond to ω_0=3.7 (-2.7) with d_1=7×10^7, 10^8 and 2.5×10^8. The dotted curve shows n_{e0}/n_0. With increasing d_1, the electron density gradient is changed more by the RMP as predicted by the analytical results. As $d_1=\omega_{ce}/\nu_e\sim T_e^{3/2}/n_e$ and T_e usually increases with decreasing n_e for a constant heating power, the value of d_1 is larger for a lower density plasma, leading to a bigger change in the electron density in this case as seen in the experiments [15].

The effect of the perpendicular particle diffusivity on the $n_{e,0/0}/n_0$ profile in steady state is shown in figure 5 for ψ_a=1×10^{-4}. The solid (dashed) curves are for ω_0=3.7 (-2.7), with $D_{\perp N}$=10, 20 and 30, where $D_{\perp N}=D_\perp/(a^2/\tau_R)$. The dotted curve shows n_{e0}/n_0. The change in the local density gradient is larger for a smaller $D_{\perp N}$, corresponding to Eq. (9) that $(\Delta n_e)'\sim d_1/D_\perp$. For the case with $D_{\perp N}$=20, $d_1/D_{\perp N}=1.25\times10^7$, corresponding to a electron density $n_e=10^{19}m^{-3}$ for $D_\perp=0.1m^2/s$ and

B_{0t}=2.5T or to a higher electron density for a stronger toroidal field, as $d_l/D_{\perp N}$ is proportional to $B_{0t}/(n_eD_\perp)$. According to Ref. 1, 15 and 16, the experimental values of the local electron density is around $10^{19}m^{-3}$.

Eq. (9) can be written in the form

$$r_s(\Delta n_e)'/n_e=(\chi_{\parallel}/D_\perp)(1-\omega_0)|b_{1r}/B_{0t}|^2(r_s/L_{pe}), \qquad (14)$$

where $\chi_{\parallel}=v_{Te}^2/\nu_e$, v_{Te} is the electron thermal velocity, and $L_{pe}=P_e/P_e'$ is the scale length of the electron pressure gradient. The change in the density gradient is larger for a higher electron temperature and a lower plasma density. For the tokamak edge plasma like that of TEXTOR with T_e=300eV, $n_e=2\times10^{19}m^{-3}$, $(1-\omega_0)$=-2, L_{pe}=a, $D_\perp=0.1m^2/s$, and $|b_{1r}/B_{0t}|=2\times10^{-5}$ at $r=r_s$, one finds $(\Delta n_e)'/n_e$=-2.2/a. For a fusion reactor like ITER with assumed local values T_e=1keV, $n_e=10^{20}m^{-3}$ and other parameters as mentioned above, $(\Delta n_e)'/n_e$=-8.9/a. Eq. (14) is subject to the limitation given by (12), so that $(\Delta n_e)'/n_e$ can be significant only for a small or moderate values of $|b_{1r}/B_{0t}|$. Once (12) is violated, the dominant change caused by RMPs is in the plasma rotation frequency [10].

The strongest improvements in particle confinement by RMPs is observed on TEXTOR in low density, low collisionality and well heated plasmas with neutral beam injection in the plasma current (ion drift) direction [15], being consistent with our theoretical results. In addition, the island width is small with high mode numbers ($m\approx6$) of the applied RMPs [15], as required by (12). Our results provide another possible explanation for the experimental results.

Since the required RMP amplitude for changing the density gradient is quite small, it would be of interest to study whether the tokamak particle confinement is affected by RMPs from intrinsic machine error field. Eq. (8) further suggests that an applied RMP of an appropriate frequency and amplitude can be utilized to either increase or decrease the local electron density gradient.

In summary, the effect of an externally applied RMP of a single helicity on the particle transport is investigated based on two fluid equations. A sufficiently large RMP is found to flatten

the local electron density profile around the rational surface as expected. With a small or moderate RMP, however, the electron density is increased if the plasma rotates in the plasma current direction with a frequency being larger than the electron drift frequency. In the opposite limit the electron density is decreased, and its local gradient may even become positive for a given constant perpendicular particle diffusivity.

References

[1] T.C. Hender, et al, Nucl. Fusion **32**, 2091 (1992).

[2] R.J. Buttery, et al, Nucl. Fusion **40**, 807 (2000).

[3] R.J. La Haye, R. Fitzpatrick, T.C. Hender et al., Phys. Fluids B **4**, 2098 (1992).

[4] S.W. Wofle, I.H. Hutchinson, R.S. Granetz et al., Phys. Plasmas **12**, 056110 (2005).

[5] H.R. Koslowski, Y. Liang A. Krämer-Flecken et al., Nucl. Fusion **46**, L1 (2006).

[6] R. Fitzpatrick, Nucl. Fusion **33**, 1049 (1993).

[7] F. L. Waelbroeck, Phys. Plasmas **10**, 4040 (2003).

[8] Q. Yu, S. Günter, Y. Kikuchi, and K. H. Finken, Nuclear Fusion **48**, 024007 (2008).

[9] K.H. Finken, S.S. Abdullaev, M.F.M. De Bock et al., Phys. Rev. Letts, **94**, 015003(2005).

[10] Q. Yu, S. Günter and K.H. Finken, Phys. Plasmas **16**, 042301 (2009).

[11] M.F.F. Nave and J.A. Wesson, Nucl. Fusion **30**, 2575 (1990).

[12] H. Zohm, A. Kallenbach, H. Bruhns, et al, Europhys. Lett. **11**, 745 (1990).

[13] Q. Yu and S. Günter, Nucl. Fusion **48**, 065004 (2008).

[14] T.E. Evans, R.A. Moyer, P.R. Thomas, et al., Phys. Rev. Letts, **92**, 235003 (2004).

[15] K.H. Finken, S.S. Abdullaev, M.W. Jakubowski et al., Phys. Rev. Letts, **98**, 065001(2007).

[16] T.E. Evans, M. Goniche, A. Grosman, et al., J. Nucl. Mater., **196&198**, 421 (1992).

[17] Q. Yu, S. Günter and Bruce D. Scott, Phys. Plasmas **10**, 797(2003).

CAPTION

Figure 1 Radial profiles of $(\Delta n_e)'/(n_0/a)$ for (1) $\omega_0 \equiv -\omega_{E0}/\omega_{*e0}=3.7$ with $\psi_a=2.54\times10^{-5}$, and (2) $\omega_0=-2.7$ with $\psi_a=2.9\times10^{-5}$. The solid curves are the full numerical results, and the dotted curves are obtained from Eq. (6) with numerical results for b_{1r} and j_1. The dashed curve shows $n_{e0}'/(n_0/a)$.

Figure 2 Radial profiles of $n_{e,0/0}/n_0$ in steady state for $\omega_0=3.7$ with $\psi_a=2.54\times10^{-5}$, 10^{-4}, 2×10^{-4}, 6×10^{-4} (solid curves) and 0 (dotted).

Figure 3 Radial profiles of $n_{e,0/0}/n_0$ in steady state for $\omega_0=-2.7$ with $\psi_a=2.9\times10^{-5}$, 3×10^{-5}, 10^{-4}, and 6×10^{-4} (solid curve) and 0 (dotted).

Figure 4 Radial profiles of $n_{e,0/0}/n_0$ in steady state for $\omega_0=3.7$ (solid) and -2.7 (dashed), with $d_1=7\times10^7$, 10^8 and 2.5×10^8, and $\psi_a=10^{-4}$. The dotted curve shows n_{e0}/n_0.

Figure 5 Radial profiles of $n_{e,0/0}/n_0$ in steady state for $\omega_0=3.7$ (solid) and -2.7 (dashed), with with $D_\perp=10$, 20 and 30 (a^2/τ_R), and $\psi_a=10^{-4}$. The dotted curve shows n_{e0}/n_0.

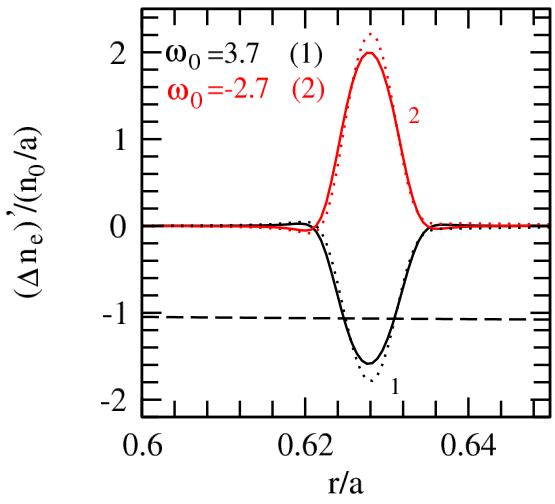

Figure 1

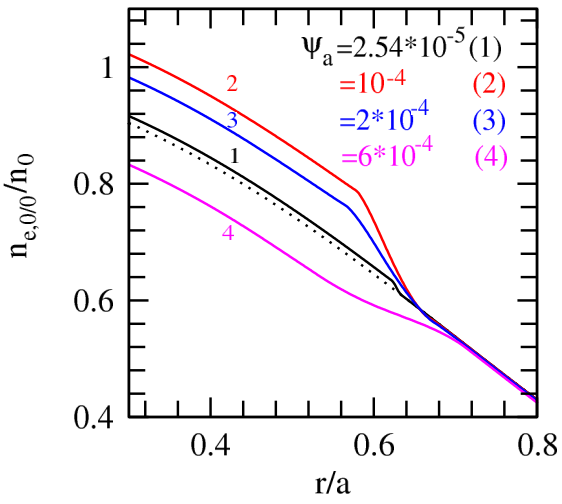

Figure 2

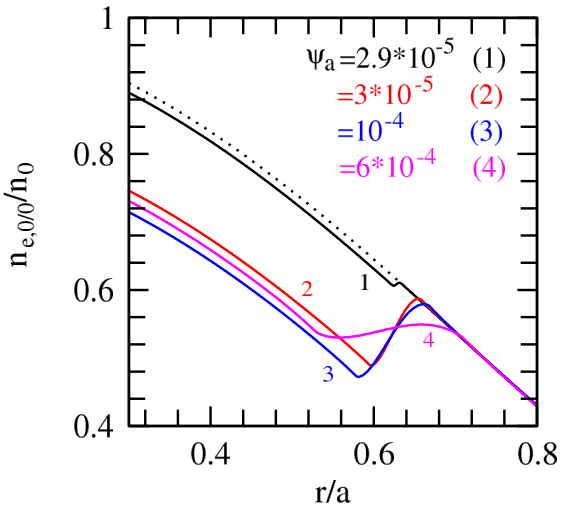

Figure 3

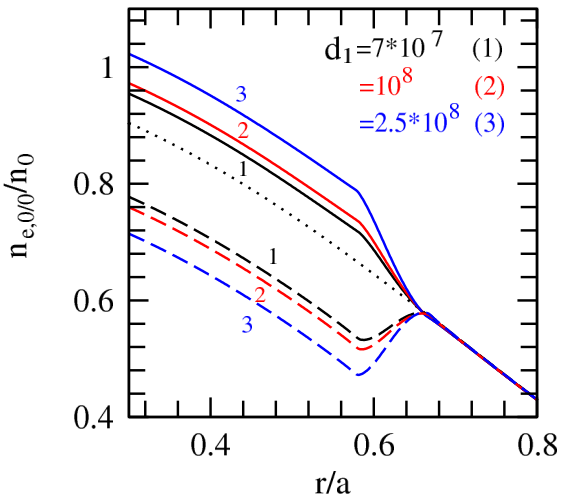

Figure 4

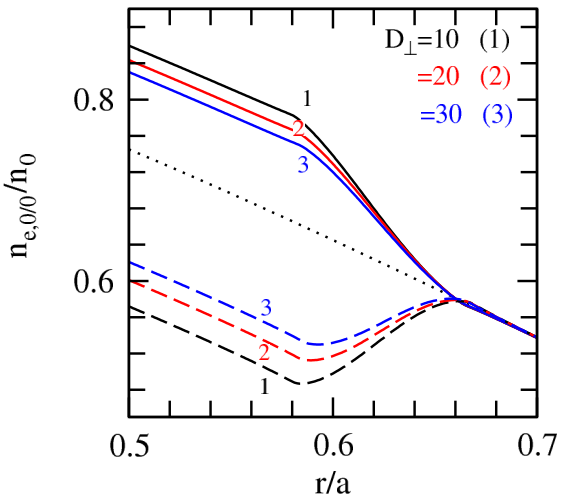

Figure 5